BESIII track fitting algorithm*

WANG Ji-Ke(王纪科)[1,2;1)] MAO Ze-Pu(毛泽普)[1;2)] BIAN Jian-Ming(边渐鸣)[1,2] CAO Guo-Fu(曹国富)[1,2]
CAO Xue-Xiang(曹学香)[1,2] CHEN Shen-Jian(陈申见)[4] DENG Zi-Yan(邓子艳)[1]
FU Cheng-Dong(傅成栋)[3,1] GAO Yuan-Ning(高原宁)[3] HE Kang-Lin(何康林)[1] HE Miao(何苗)[1]
HUA Chun-Fei(花春飞)[5] HUANG Bin(黄彬)[1,2] HUANG Xing-Tao(黄性涛)[10] JI Xiao-Bin(季晓斌)[1]
LI Fei(李飞)[1] LI Hai-Bo(李海波)[1] LI Wei-Dong(李卫东)[1] LIANG Yu-Tie(梁羽铁)[6]
LIU Chun-Xiu(刘春秀)[1] LIU Huai-Min(刘怀民)[1] LIU Suo(刘锁)[7] LIU Ying-Jie(刘英杰)[1]
MA Qiu-Mei(马秋梅)[1] MA Xiang(马想)[1,2] MAO Ya-Jun(冒亚军)[6] MO Xiao-Hu(莫晓虎)[1]
PAN Ming-Hua(潘明华)[8] PANG Cai-Ying(庞彩莹)[8] PING Rong-Gang(平荣刚)[1] QIN Ya-Hong(秦亚红)[5]
QIU Jin-Fa(邱进发)[1] SUN Sheng-Sen(孙胜森)[1] SUN Yong-Zhao(孙永昭)[1] WANG Liang-Liang(王亮亮)[1,2]
WEN Shuo-Pin(文硕频)[1] WU Ling-Hui(伍灵慧)[1] XIE Yu-Guang(谢宇广)[1] XU Min(徐敏)[9]
YAN Liang(严亮)[1,2] YOU Zheng-Yun(尤郑昀)[6] YUAN Chang-Zheng(苑长征)[1] YUAN Ye(袁野)[1]
ZHANG Bing-Yun(张炳云)[1] ZHANG Chang-Chun(张长春)[1] ZHANG Jian-Yong(张建勇)[1]
ZHANG Xue-Yao(张学尧)[10] ZHANG Yao(张瑶)[1] ZHENG Yang-Heng(郑阳恒)[2] ZHU Ke-Jun(朱科军)[1]
ZHU Yong-Sheng(朱永生)[1] ZHU Zhi-Li(朱志丽)[8] ZOU Jia-Heng(邹佳恒)[10]

1 (Institute of High Energy Physics, CAS, Beijing 100049, China)
2 (Graduate University of Chinese Academy of Sciences, Beijing 100049, China)
3 (Tsinghua University, Beijing 100084, China)
4 (Nanjing University, Nanjing 210093, China)
5 (Zhengzhou University, Zhengzhou 450001, China)
6 (Peking University, Beijing 100871, China)
7 (Liaoning University, Shenyang 110036, China)
8 (Guangxi Normal University, Guilin 541004, China)
9 (Department of Modern Physics, University of Science and Technology of China, Hefei 230026, China)
10 (Shandong University, Jinan 250100, China)

Abstract A track fitting algorithm based on the Kalman filter method has been developed for BESIII of BEPCII. The effects of multiple scattering and energy loss when the charged particles go through the detector, non-uniformity of magnetic field (NUMF) and wire sag, etc., have been carefully handled. This algorithm works well and the performance satisfies the physical requirements tested by the simulation data.

Key words BESIII main drift chamber, track fitting algorithm, Kalman filter method

PACS 07.05.Fb, 07.05.Tp

1 Introduction

BESIII is a high precision general purpose detector which is designed for the high luminosity e^+e^- collider BEPCII running in the tau-charm energy region. The BESIII detector consists of the following sub-systems: the main drift chamber (MDC), the time of flight counter (TOF), the electromagnetic calorimeter (EMC), the muon counter (MUC) and the super-conducting magnet, etc. The physics programs of the BESIII experiment require highly accurate track parameters near both the interaction point

Received 12 January 2009, Revised 4 May 2009

* Supported by CAS Knowledge Innovation Project(U-602, U-34), National Natural Science Foundation of China (10491300, 10491303, 10605030) and 100 Talents Program of CAS (U-25, U-54)

1) E-mail: wangjk@ihep.ac.cn

2) E-mail: maozp@ihep.ac.cn

and the outermost layer of MDC.

MDC is the most important and the unique tracking sub-detector of BESIII; it is used to precisely determine the track momentum, direction and vertex position of charged particles. MDC consists of an inner chamber without an outer wall and an outer chamber without an inner wall, which are jointed by 6 stepped end flanges. The inner radius and outer radius of the chamber are 64 and 810 mm. The length ranges from 774 mm for the innermost layer to 2400 mm for the outermost layer. It is symmetrical in the z direction to cover the polar angle region of $-0.93\leqslant\cos\theta\leqslant0.93$. The wires of MDC are arranged in 43 layers, which are 8 stereo layers, 12 axial layers, 16 stereo layers and 7 axial layers going from inside to outside. The small drift cell structure of the inner chamber has dimensions of 6 mm × 6 mm and the outer of 8 mm × 8 mm. The single wire spatial resolution and $\mathrm{d}E/\mathrm{d}x$ resolution are expected to be 130 μm and 6% respectively[1].

In BESIII offline reconstruction software[2], there are two track finding algorithms, which are TrkReco[3] and MdcPatRec[4]. The main task of them is to find out the useful hits and tracks in high speed and good efficiency. In this first stage of tracking, the charged particle trajectory moving in the detector is described with a standard helix; the material effects, NUMF and some other detailed corrections have not been taken into account.

When a charged particle moves in a uniform magnetic field its trace is a standard helix. The particle trajectory is a function of some initial parameters such as its momentum and position when it is produced. Generally speaking, the task of track fitting is to determine these initial parameters from a set of measurements along the track. If a particle does not interact with material, an optimal estimate of the initial parameters can be given by a global χ^2-fit to the measurements. However, if there is material along the track and the magnetic field is not uniform, the global χ^2-fit is not suitable. Therefore, we introduce the Kalman filter method to do it[5, 6].

The Kalman filter method is widely used in many science and technology fields. It was introduced by Kalman[7], and was applied to high energy physics experiment in the 80s by Frühwirth[8] and Billoir[9], then it becomes very popular in this challenging domain[10—14]. There are lots of Kalman filter application examples such as pattern recognition[15], detector alignment[16], vertex finding and particle identification[17],etc.

The basic principle and formulations of a Kalman filter can be found in many textbooks with different generalizations[18, 19]. The notations and conventions of Frühwirth are adopted to describe it here[8, 20]. In a discrete linear dynamics system, the evolution of the state vector at time k x_k is expressed with a linear transformation plus a random perturbation w:

$$x_k = F_{k-1}x_{k-1} + w_{k-1}\,. \tag{1}$$

In this equation, F is the propagation matrix.

The measurement m_k can be written as a linear function of the state vector:

$$m_k = H_k x_k + \epsilon_k\,. \tag{2}$$

This equation is called the measurement equation and the matrix H is called the project matrix.

The evolution of the state vector may proceed in space or in time, or along a dimensionless integer, etc. Define:

$$\begin{gathered}\mathrm{cov}\{w_k\} = Q_k,\ \ \mathrm{cov}\{\epsilon_k\} = V_k = G_k^{-1}\,,\\ C_k^i = \mathrm{cov}\{x_k^i - x_{k,\mathrm{true}}\}\,.\end{gathered} \tag{3}$$

Here $x_{k,\mathrm{true}}$=true value of the state vector at time k. x_k^i=estimation of using measurements up to time i ($i<k$: prediction, $i=k$: filtering, $i>k$: smoothing). x_k^k is simplified as x_k below. Then the three parts of a complete Kalman filter system can be written as:

1) Prediction: the estimation of the state vector at "future" time $k+1$ with information at k.

Extrapolation of state vector:

$$x_k^{k-1} = F_{k-1}x_{k-1}\,. \tag{4}$$

Extrapolation of covariance matrix:

$$C_k^{k-1} = F_{k-1}C_{k-1}F_{k-1}^{\mathrm{T}} + Q_{k-1}\,. \tag{5}$$

Residuals of prediction:

$$r_k^{k-1} = m_k - H_k x_k^{k-1}\,. \tag{6}$$

2) Filtering: the estimation of the present state vector at k with all past measurements until $k-1$.

Update of state vector in filtering:

$$x_k = x_k^{k-1} + K_k(m_k - H_k x_k^{k-1})\,. \tag{7}$$

K_k is the "Kalman gain matrix". Its expression is:

$$K_k = C_k^{k-1}H_k^{\mathrm{T}}(V_k + H_k C_k^{k-1}H_k^{\mathrm{T}})^{-1} = C_k H_k^{\mathrm{T}} G_k\,. \tag{8}$$

Update of covariance matrix:

$$C_k = [(C_k^{k-1})^{-1} + H_k^{\mathrm{T}}G_k H_k]^{-1}\,. \tag{9}$$

Residuals of filtering:

$$r_k = m_k - H_k x_k = (I - H_k K_k)r_k^{k-1}\,. \tag{10}$$

Increment of χ^2:

$$\chi_+^2 = r_k^{\mathrm{T}}R_k^{-1}r_k\,. \tag{11}$$

Here R_k is the covariance of the filtered residuals:

$$R_k = (I - H_k K_k)V_k = V_k - H_k C_k H_k^{\mathrm{T}} . \quad (12)$$

3) Smoothing: a backward estimation of the state vector at k with all measurements $n(>k)$.

The smoothed state vector:

$$x_k^n = x_k + A_k(x_{k+1}^n - x_{k+1}^k) . \quad (13)$$

Here A_k is the smoothing gain matrix:

$$A_k = C_k F_k^{\mathrm{T}} (C_{k+1}^k)^{-1} . \quad (14)$$

Covariance matrix:

$$C_k^n = C_k + A_k(C_{k+1}^n - C_{k+1}^k)A_k^{\mathrm{T}} . \quad (15)$$

Smoothed residuals:

$$r_k^n = r_k - H_k(x_k^n - x_k) = m_k - H_k x_k^n . \quad (16)$$

The application of the Kalman filter method to track fitting is straightforward if a track in space is considered as a dynamic system. This method updates the fitting results in each step with the addition of measurement points, then it deals with multiple scattering, energy loss and NUMF as a deviation with a Gaussian distribution in each step[14], to yield more accurate track parameters and error matrix.

In the magnetic field, a charged particle track in a detector can be described with five independent parameters at each point. The vector of track parameters can be interpreted as the state vector x of the dynamic system. If z is the growth parameter of the track (such as time), $x = x(z)$ describes the whole track. The evolution of the system is determined by the system equation:

$$x(z_k) = f_{k-1}(x_{k-1}) + w_{k-1} . \quad (17)$$

f_{k-1} is the propagator for the track from measurement $k-1$ to measurement k, w_{k-1} is the random noise from $k-1$ to k. The measurement value at k is m_k and the measurement noise (error) is denoted with ϵ_k. Then $m_k = h_k(x_k) + \epsilon_k$ is the measurement function.

2 Task and challenge of BESIII track fitting

In BESIII, the materials affecting the particle trajectory mainly include the matters in the beam pipe and the gas in the drift chamber. The beam pipe consists of two beryllium layers with 0.8 mm cooling oil between them. The inner layer diameter is 63 mm with a thickness of 0.8 mm, while the thickness of the outer layer is 0.6 mm. There is a 14 μm gold coating on the inside of the beryllium pipe. For the main drift chamber, in order to reduce the effect of multiple scattering, a helium based gas (60% helium and 40% propane) is chosen as the working gas. In the MDC tracking region, the nominal magnetic field value is 1.0 Tesla and the direction is along the minus z-axis. But in real situations, the magnetic field is non-uniform and the degree of non-uniformity is about 10%[21]. Simulation results show that this non-uniformity effect has an even more significant influence on the track finding result than material effects. There are 6796 sense wires of MDC; due to gravity and electrostatic forces, the wires' positions deviate from the ideal positions, then the calculated minimal distance between the track and the sense wire will be affected. The average maximal sagitta of the wires is about 100 μm. All of the materials, NUMF and wire sagitta effects will be corrected in the fitting algorithm.

2.1 Track model

The track model in the Kalman filter track fitting adopts five parameters $a \equiv (d_\rho, \phi_0, \kappa, d_z, \tan\lambda)^{\mathrm{T}}$ to describe the track[22], the geometrical meaning of the parameters is described in Fig. 1.

1) d_ρ is the signed distance of the helix from the pivot in x-y plane. Sometimes d_ρ can also be written as d_{r} or d_0.

2) ϕ_0 is the azimuthal angle to specify the pivot with respect to the helix center.

3) κ is $1/P_{\mathrm{t}}$ (reciprocal of the transverse momentum) and the sign of κ represents the charge of the track assigned by the track fitting.

4) d_z is the signed distance of the helix from the pivot in the z direction.

5) $\tan\lambda$ is the slope of the track, the tangent of the dip angle.

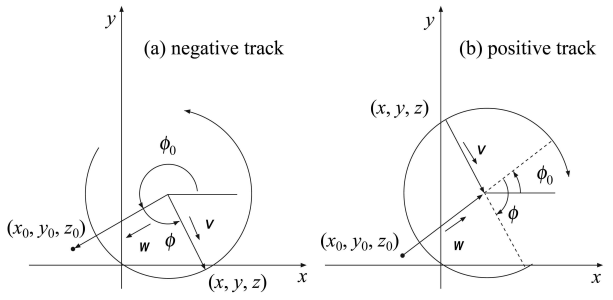

Fig. 1. Schematic representation of the helix parametrization for (a) negative and (b) positive charged track. The vectors in the figure are defined by $\boldsymbol{x} = \boldsymbol{x}_0 + (d_\rho + \rho)\cdot\boldsymbol{w} - \rho\cdot\boldsymbol{v}$, where $\boldsymbol{w} = (\cos\phi_0, \sin\phi_0)^{\mathrm{T}}$ and $\boldsymbol{v} = (\cos(\phi_0 + \phi), \sin(\phi_0 + \phi))^{\mathrm{T}}$.

2.2 Error model

The measurement covariance matrix V should represent the expected errors of the given measurements, including the errors due to both geometrical alignment and the intrinsic detector resolution. When a single coordinate (the drift distance in BESIII MDC) is measured, the measurement covariance matrix is just the variance of the measurement[23]:

$$V_{\rm meas}=\sigma^2_{\rm meas}\,. \tag{18}$$

The $\sigma_{\rm meas}$ can be obtained from double Gaussian fitting to the distribution of the residual[24]. It is calculated as:

$$\sigma_{\rm meas}=\sqrt{f\cdot\sigma_1^2+(1-f)\cdot\sigma_2^2}\,. \tag{19}$$

Here, σ_1 is the resolution of the narrower Gaussian distribution, f represents its proportion in the whole residual distribution; σ_2 is of the wider one.

2.3 Material effects

2.3.1 Multiple scattering

When a charged particle traverses matter, it is deflected by many small-angle Coulomb scatters. The Coulomb scattering distribution is well represented by the theory of Molière. It is sufficient for many applications to use a Gaussian approximation for the central 98% of the projected angular distribution, with a width[25]:

$$\theta_0=\frac{13.6\ {\rm MeV}}{\beta cp}z\sqrt{x/X_0}[1+0.038\ln(x/X_0)]. \tag{20}$$

Here p, βc, z are the momentum, velocity, charge number of the incident particle, X_0 is the radiation length of the material, and x/X_0 is the thickness of the material in units of its radiation length.

In MDC, on the track path of length l, the contribution of multiple scattering to the error matrix (to the approximation of second order of l) is[23]:

$$V_{\rm mcs}=\theta^2_{\rm mcs}\begin{pmatrix} l^2/3 & (p/p_{\rm t})l/2 & 0 & 0 & 0\\ (p/p_{\rm t})l/2 & (p/p_{\rm t})^2 & 0 & 0 & 0\\ 0 & 0 & (\kappa\tan\lambda)^2 & (p_z/p)\kappa l/2 & (p/p_{\rm t})^2\kappa\tan\lambda\\ 0 & 0 & (p_z/p)\kappa l/2 & (p_{\rm t}/p)^2l^2/3 & (p/p_{\rm t})l/2\\ 0 & 0 & (p/p_{\rm t})^2\kappa\tan\lambda & (p/p_{\rm t})l/2 & (p/p_{\rm t})^4 \end{pmatrix}, \tag{21}$$

where p, $p_{\rm t}$, p_z are the total momentum, transverse momentum and z component of momentum, respectively. κ and $\tan\lambda$ are two track parameters. $\theta_{\rm mcs}$ is the same as θ_0 mentioned above.

2.3.2 Energy loss

Charged particles other than electrons lose energy in matter mainly by ionization and atomic excitation. The mean rate of energy loss (or stopping power) is described by Bethe-Bloch equation:

$$-\frac{{\rm d}E}{{\rm d}x}=Kz^2\frac{Z}{A}\frac{1}{\beta^2}\left[\frac{1}{2}\ln\frac{2m_{\rm e}c^2\beta^2\gamma^2T_{\rm max}}{I^2}-\beta^2-\frac{\delta(\beta\gamma)}{2}\right]. \tag{22}$$

A detailed explanation of this equation can be seen in the Particle Data Group[25, 26].

If the particle loses a small amount of energy ΔE, the trajectory of the track will be affected and the track parameter κ is updated as:

$$\kappa'=\kappa\frac{p}{\sqrt{p^2+2E\Delta E+\Delta E^2}}\,. \tag{23}$$

As there is straggling in the energy loss, it is not deterministic. Let $\sigma_{\Delta E}$ denote the mean squared value of the straggling of ΔE. The straggling will add a contribution to the error matrix elements. The modification to matrix element V_{kk} is:

$$V'_{kk}=V_{kk}+\frac{\kappa^2E^2}{p^4}\sigma^2_{\Delta E}\,. \tag{24}$$

The curvature of the track will be changed when it loses some energy; this will also affect the error matrix due to a pure geometrical effect. The update of the error matrix is:

$$\begin{cases} V'_{\kappa\kappa}=a^2V_{kk}+2abV_{\kappa\tan\lambda}+b^2V_{\tan\lambda\tan\lambda}\\ V'_{\kappa\phi_0}=aV_{\kappa\phi_0}+bV_{\tan\lambda\phi_0}\\ V'_{\kappa d_\rho}=aV_{\kappa d_\rho}+bV_{\tan\lambda d_\rho}\\ V'_{\kappa\tan\lambda}=aV_{\kappa\tan\lambda}+bV_{\tan\lambda\tan\lambda}\\ V'_{\kappa d_z}=V_{\kappa d_z}+bV_{\tan\lambda d_z} \end{cases}. \tag{25}$$

Here a and b are:

$$\begin{cases} a\equiv\dfrac{\partial\kappa'}{\partial\kappa}=\dfrac{\kappa'^3E'}{\kappa^3E}\\ b\equiv\dfrac{\partial\kappa'}{\partial\tan\lambda}=\dfrac{\tan\lambda}{1+\tan^2\lambda}\kappa'\left(1-\dfrac{\kappa'^2E'}{\kappa^2E}\right) \end{cases}. \tag{26}$$

2.4 Non-uniformity of magnetic field

In the track fitting algorithm, the track parameters are transported with nominal magnetic field (1.0

Tesla in the minus z direction), treating the NUMF as perturbation. The initial track is divided into many small pieces: the more inhomogeneous, the shorter the piece. For each piece, the modification to the momentum due to NUMF can be calculated as a path integral[27, 28]:

$$\Delta\boldsymbol{p}=\int_{l_0}^{l_1}(\boldsymbol{B}_{\rm true}-\boldsymbol{B}_{\rm nom.})\times{\rm d}\boldsymbol{l}\,. \tag{27}$$

According to the relation between the particle momentum and track parameters:

$$\begin{cases} P_x=-\dfrac{\sin(\phi_0+\phi)}{|\kappa|} \\ P_y=\dfrac{\cos(\phi_0+\phi)}{|\kappa|} \\ P_z=\dfrac{\tan\lambda}{|\kappa|} \end{cases}. \tag{28}$$

We can get:

$$\begin{cases} \Delta P_x=-\dfrac{\Delta\kappa}{|\kappa|}P_x-\Delta\phi_0 P_y \\ \Delta P_y=-\dfrac{\Delta\kappa}{|\kappa|}P_y+\Delta\phi_0 P_x \\ \Delta P_z=\dfrac{\Delta\kappa}{|\kappa|}P_z+\dfrac{\Delta\tan\lambda}{|\kappa|} \end{cases}. \tag{29}$$

Solving the equation in (29), the change of track parameters is:

$$\begin{cases} \Delta\phi_0=|\kappa|(\Delta P_y\cos\phi_0-\Delta P_x\sin\phi_0) \\ \Delta\kappa=|\kappa|\kappa(\Delta P_x\cos\phi_0+\Delta P_y\sin\phi_0) \\ \Delta\tan\lambda=\Delta P_z|\kappa|+\dfrac{\tan\lambda\Delta\kappa}{\kappa} \end{cases}. \tag{30}$$

2.5 Wire sag effect

Another important effect handled in the fitting algorithm is the wire sagitta. Under gravity and electrostatic forces, the balance equation of the sense wire is:

$$T({\rm d}^2y/{\rm d}z^2)+ky+g\rho\sigma=0\,. \tag{31}$$

Here z is along the direction of the wire, $y(z)$ is the vertical displacement. T is the tension, k is the coefficient of the electrostatic force, g is gravitational acceleration, ρ and σ are the density and cross section of the wire. L is the length of the wire. Ignoring the electrostatic force, $k=0$ is set to solve the equation giving:

$$y(z)=\frac{g\rho\sigma}{T}(zL-z^2)\,. \tag{32}$$

The sag of the wire is defined as the sag distance at the middle point of the wire:

$$S_{\rm g}=y\left(\frac{L}{2}\right)=\frac{L^2g\rho\sigma}{8T}\,. \tag{33}$$

3 Design and implementation of the algorithm

In the BESIII Offline Software System (BOSS)[2], the interface and communication are totally defined by the data exchange. The event data model (EDM) for the drift chamber simultaneously considers the needs from calibration, track finding and track fitting. For KalFitAlg, the input collection RecMdcTrackCol contains the reconstructed tracks and the hit information from the track finding. The interfaces of the two independent pattern recognition algorithms to KalFitAlg are the same as guaranteed by the EDM. The output of KalFitAlg is modeled as RecMdc-KalTrackCol, which contains the fitted track information which is required by succedent algorithms. During offline event reconstruction, data converters in the BOSS framework convert raw data on various media and register them into the Transient Data Store (TDS). Various algorithms use the Event Data Service to visit the data. The reconstruction results are registered into TDS also, with the format defined by the EDM.

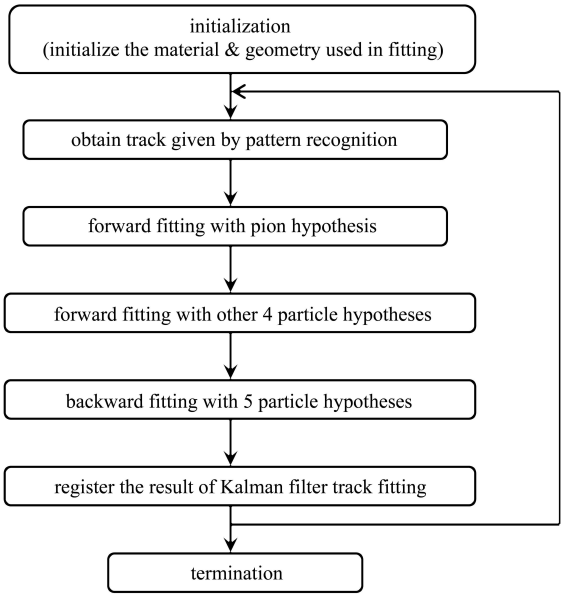

Fig. 2. The flow of KalFitAlg.

In KalFitAlg, we firstly initialize the geometrical configurations and material properties of MDC and the beam pipe, and also fetch the BESIII magnetic field map. Then the tracks collection which are given by track finding are obtained. For each track, in the beginning, we do forward fitting with five particle hypotheses (e, μ, π, k, p) to give the fitting results at the interaction point (IP). According to the control options in the user's job file, the backward fitting can

also be selected to give the fitting results at the outermost hit layer of MDC. Finally, the fitted tracks are registered into TDS for the next physics tool or analysis people to use. The whole flow can be seen in Fig. 2.

3.1 Starting of the algorithm

The initial track parameters and error matrix are needed to start the track fitting algorithm. The initial track parameters can be got from the track finding. But the initial error matrix is hard to decide, as it cannot be too big or too small. If it is set too big, the fitting may not converge well and affect the final resolution of the parameters. In some situation, such as for low momentum particles, the seeds of the fitting algorithm deviate from the truth a lot and it is unreliable; in order to avoid biasing the final fitting result, a large enough initial error matrix is required.

3.2 Hit discarding in the track fitting

When adding a measurement hit to a track, the contribution of the hit to the total fitting χ^2 is chosen as the criterion to decide whether to keep this hit in the track's hit collection. The χ^2 distribution of the hits at every layer has been studied to decide the cuts in filtering and smoothing. Two typical distributions are shown in the following figures (Fig. 3) and the black arrows in the figures point to the cut values actually used in the filtering and smoothing of the algorithm.

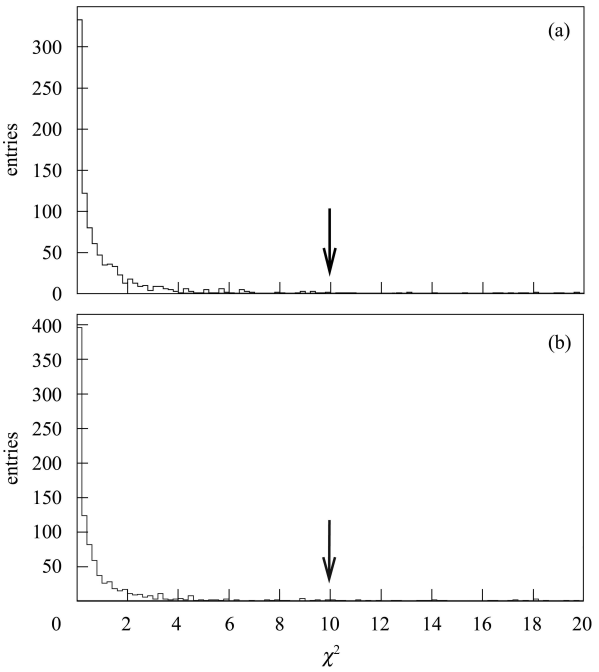

Fig. 3. (a) The typical χ^2 contribution of hits in filtering; (b)The typical χ^2 contribution of hits in smoothing.

4 Preliminary check of the package

For evaluating the performance of KalFitAlg, some checks have been done with simulation data samples. This part will show and analyze the efficiency and performance of this fitting algorithm.

4.1 The efficiency

The efficiency of the track fitting algorithm is defined as:

$$\epsilon = \frac{N_{\rm good}}{N_{\rm rec}}, \tag{34}$$

where $N_{\rm good}$ is the number of the tracks which can be successfully fitted in the KalFitAlg, and $N_{\rm rec}$ is the number of tracks given by track finding. We studied the efficiency with different momenta and different polar angle situations with two kinds of data samples. The first kind of data is a 1.0 GeV single proton with $\cos\theta$ ranging from -0.90 to 0.90 and the second is a single proton with different momenta but a fixed polar angle at $\cos\theta$=0.90. We can see from Fig. 4 that in most cases, the efficiency is about 99%, except that when the $|\cos\theta|$ is very big or the proton momentum is fairly low, the efficiency drops slightly to 95%.

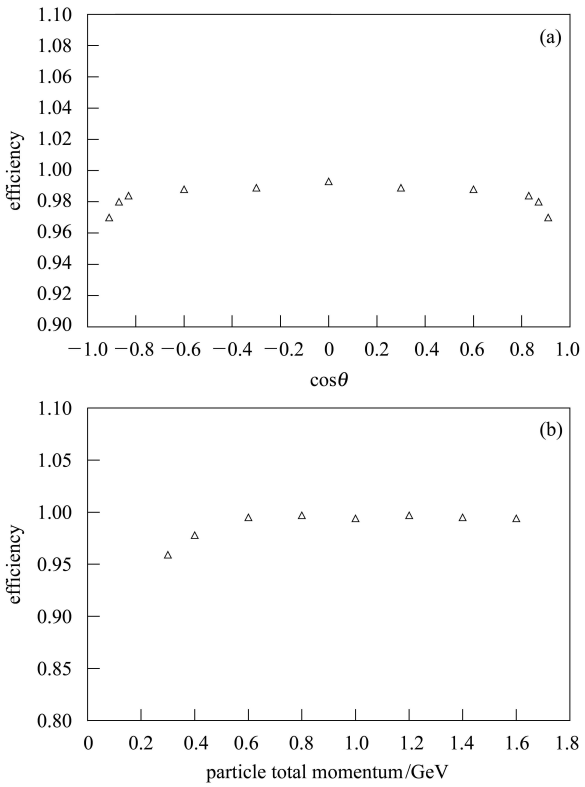

Fig. 4. Kalman filter track fitting efficiency study. (a) The efficiencies for a 1.0 GeV single proton with different $\cos\theta$; (b)The efficiencies for a single proton with different momenta and a fixed polar angle at $\cos\theta$=0.90.

4.2 Discussion of the efficiency

The decline at some track angle and momentum regions may be caused by some reasons. The first one is that when the particle momentum is very low and in the big $|\cos\theta|$ region, the material and NUMF effects affect the precision of the track finding dramatically, so the initial seeds including the track parameters and the left/right decision of the hits obtained from track finding are not very good. The second one is that because the initial error matrix chosen may not be very suitable in this situation, more adjustments are needed to get the optimal results. The third one is that the magnetic field of MDC is most inhomogeneous in this region, the approximate treatment of the NUMF used in this algorithm and the step length of every helix piece should be carefully checked.

However, the tracks that cannot pass the fitting algorithm will not be discarded, they will still be kept and registered into TDS but with a special tag. In other words, the KalFitAlg does not lose efficiency on the track finding level.

4.3 Momentum resolution and mean value improvement

The momentum resolution before and after the Kalman filter track fitting has been compared by using single proton data samples at different momentum points. Since in the Kalman filter track fitting, the effects of multiple scattering and energy loss have been carefully treated, the momentum resolution gets much better after the fitting, especially in the low momentum situation (see Fig. 5(a)).

Also as the material and NUMF effects have been handled in the fitting, the differences between the fitted and Monte-Carlo (MC)[29] momentum values are about zero in all momentum situations (see Fig. 5(b)), which means the momentum of the particle at IP after fitting matches the MC generated value well. It also indicates that in the fitting algorithm the corrections of these effects are reasonable.

4.4 Improvement on track parameters and their error matrix

The pull distribution tells the similarity of distribution of the measured values with the standard Gaussian distribution $N(\mu,\sigma^2)$. It is the most direct test of the goodness of the track parameters and the error matrix. For a variable x, its pull distribution is defined as:

$$\text{pull}(x)=\frac{x_{\text{fit}}-x_{\text{true}}}{\sigma_x}. \tag{35}$$

The pull distributions of the 5 track parameters and the total momentum at the IP are shown in Fig. 6, and are quite similar to the standard $N(0,1)$ distribution.

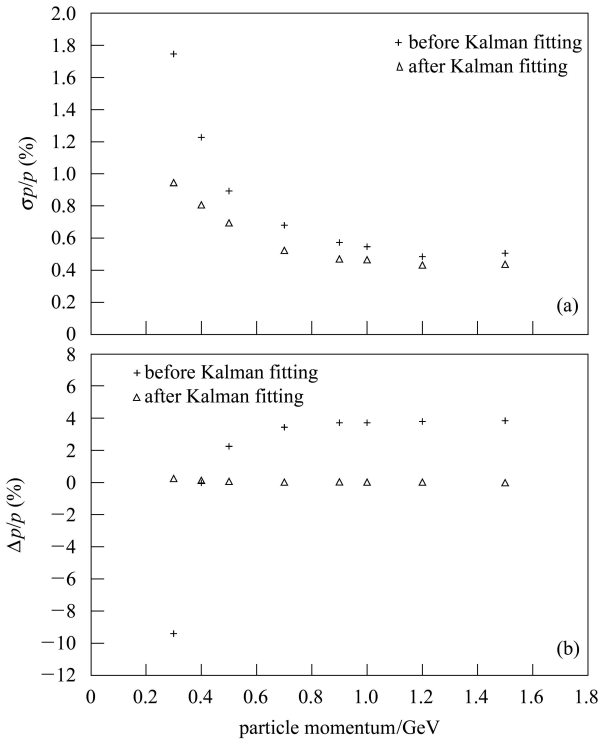

Fig. 5. (a) The momentum resolution of a single proton with different momenta, before and after the Kalman filter track fitting. (b) The difference of particle momentum with the MC input value, before and after the Kalman filter track fitting.

5 Important application in physics analysis

We have investigated the application of the Kalman filter track fitting to physics analysis by using some typical decay channels; the results showed that the Kalman filter track fitting is fairly important to physics analysis. The first channel is $\psi(2S)\to \text{J}/\psi\pi^+\pi^-$, $\text{J}/\psi\to\mu^+\mu^-$. The mass of J/ψ cannot only be got from the invariable mass of the muon pair but can also be got from the recoiling mass of the pion pair. Fig. 7(a) shows the invariant mass spectrum of $\mu^+\mu^-$, the dashed line stands for the mass distribution without the Kalman filter track fitting and the solid line for the mass distribution with the Kalman filter track fitting, whose resolution is about 10 MeV.

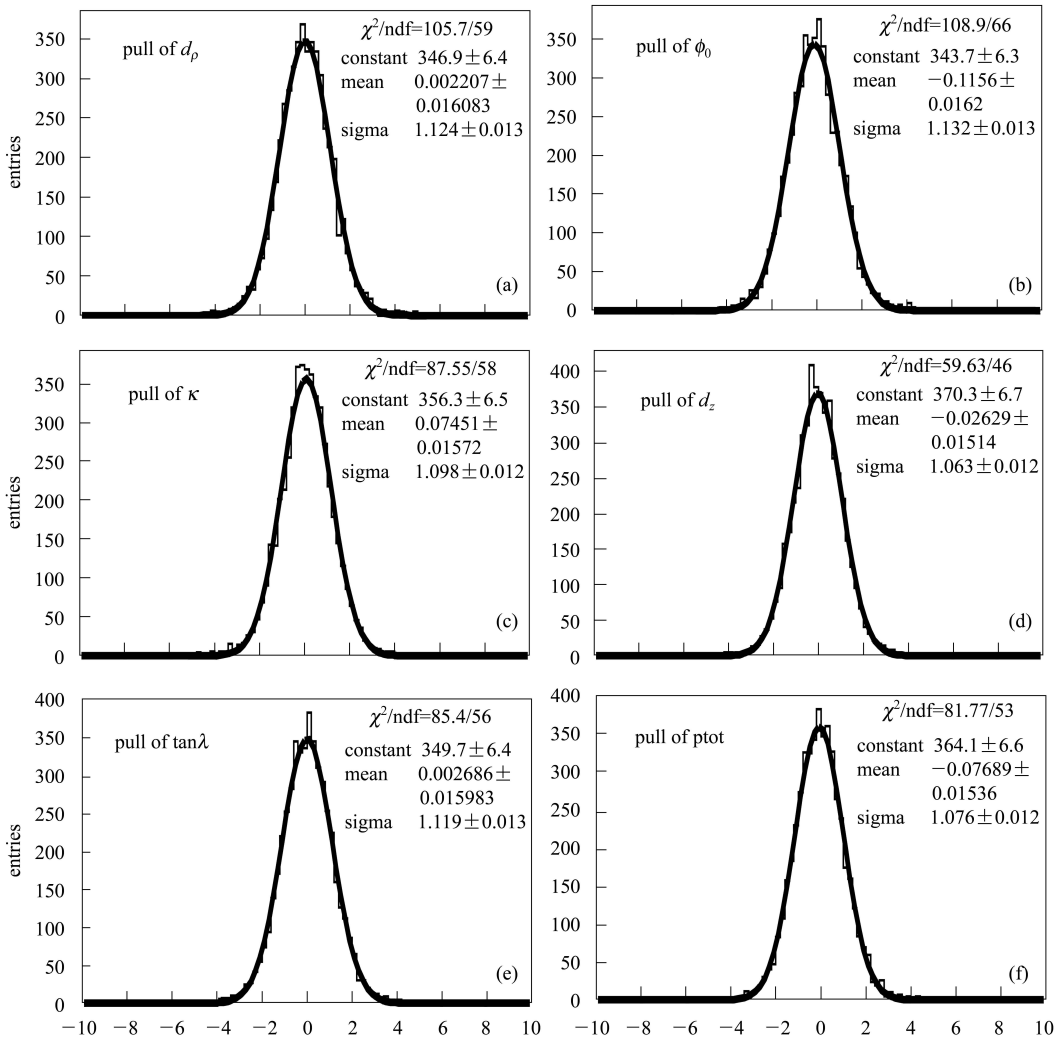

Fig. 6. The pull distributions of the 5 track parameters and the total momentum at IP. The data sample is a 1.0 GeV proton. (a) The pull distribution of the track parameter d_ρ. (b) The pull distribution of the track parameter ϕ_0. (c) The pull distribution of the track parameter κ. (d) The pull distribution of the track parameter d_z. (e) The pull distribution of the track parameter $\tan\lambda$. (f) The pull distribution of the total momentum of the particle at IP.

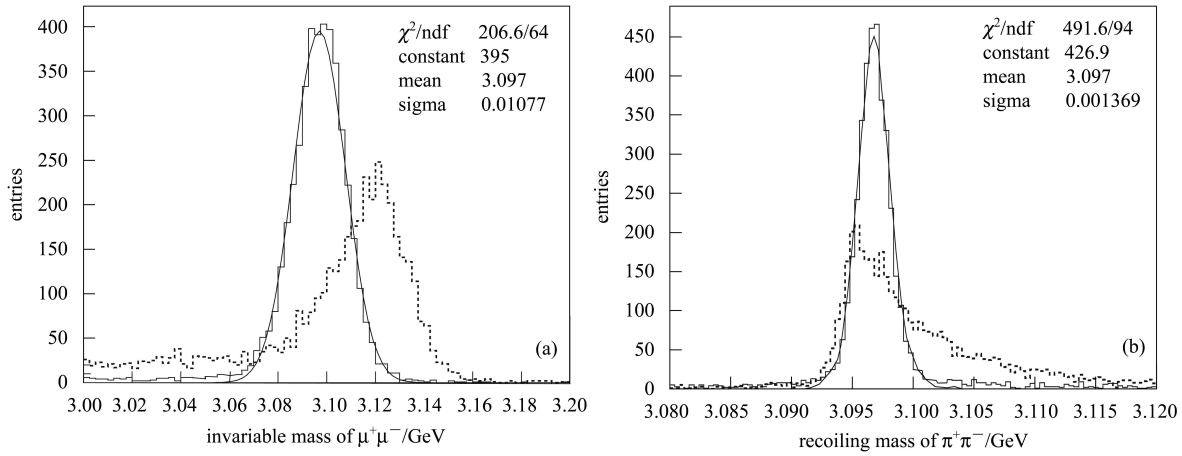

Fig. 7. The decay channel $\psi(2S)\to\pi^+\pi^- J/\psi$, $J/\psi\to\mu^+\mu^-$: (a) The invariant mass spectrum of $\mu^+\mu^-$ with and without the Kalman filter track fitting. (b) The recoiling mass spectrum of $\pi^+\pi^-$ with and without the Kalman filter track fitting.

Fig. 7(b) shows the recoiling mass spectrum of $\pi^+\pi^-$, the dashed line stands for the mass distribution without the Kalman filter track fitting and the solid line for the mass distribution with the Kalman filter track fitting, whose resolution is about 1.5 MeV. The second channel is $J/\psi \to p\bar{p}\pi^+\pi^-$, this channel is an important decay channel in J/ψ physics, in which there are many interesting resonances. The momentum of the final state proton or anti-proton is low and the moving speed of them in the detector is quite slow. So the material and NUMF effects have a big influence on the track finding result. Fig. 8 shows the invariable mass spectrum of $p\bar{p}\pi^+\pi^-$, the dashed line stands for the mass distribution without the Kalman filter track fitting and the solid line for the mass distribution with the Kalman filter track fitting. We can see clearly that the spectrum with the Kalman filter track fitting is much better than that without it.

About this $J/\psi \to p\bar{p}\pi^+\pi^-$ decay channel, the χ^2 distribution of 4C kinematic fit with and without the Kalman filter track fitting also has been compared. The result shows that the former is much more reasonable than the latter, see Fig. 9.

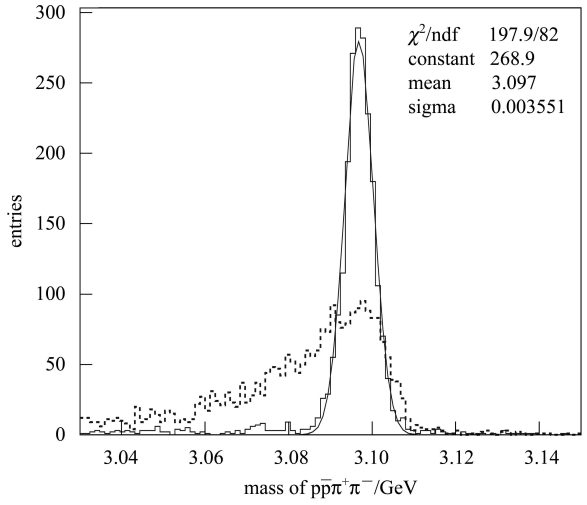

Fig. 8. The decay channel $J/\psi \to p\bar{p}\pi^+\pi^-$. The invariant mass spectrum of $p\bar{p}\pi^+\pi^-$ with and without the Kalman filter track fitting.

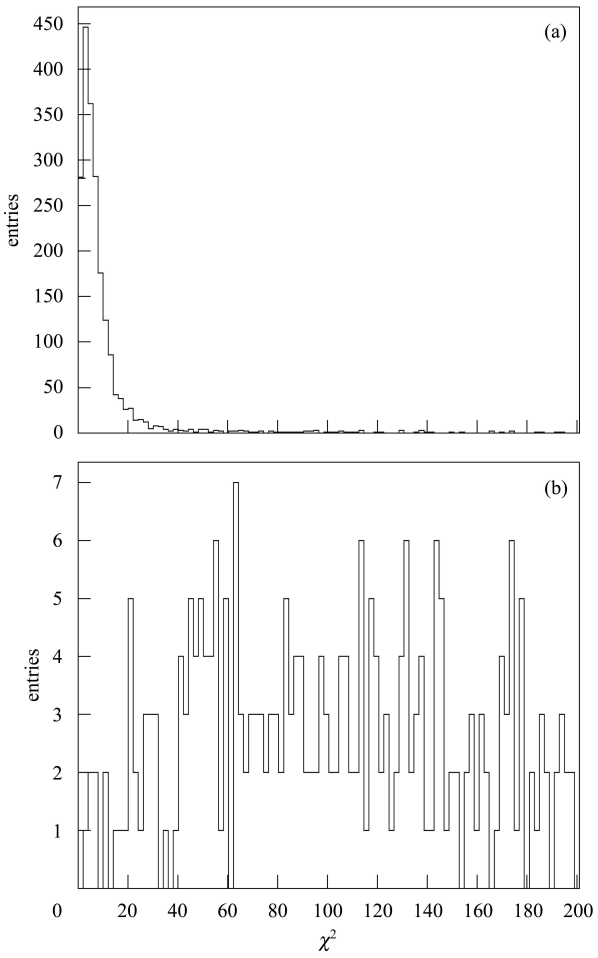

Fig. 9. The χ^2 distribution of 4C kinematic fit with (a) and without (b) the Kalman filter track fitting of channel $J/\psi \to p\bar{p}\pi^+\pi^-$. The cut of χ^2 is set at 200.

6 Summary

A track fitting algorithm based on the Kalman filter method is designed and created for BESIII at BEPC II. It works stably and the performance basically satisfies the requirements of the BESIII physics analysis, which has been checked by both simulation and true colliding data samples. We also really appreciate all the help from the Belle collaboration and thank TRAK's author, Karim Trabelsi[30].

References

1 BEPC II TDR, detector part. 2003 (in Chinese)
2 http://boss.ihep.ac.cn
3 LIU Qiu-Guang et al. Chin. Phys. C (HEP & NP), 2008, **32**(7): 565—571
4 ZHANG Yao et al. HEP & NP, 2007, **31**(6): 570—575 (in Chinese)
5 Avery P. Applied Fitting Theory IV, Formulas for Track Fitting. CBX 92-45, 1992
6 Avery P. Applied Fitting Theory V, Track Fitting Using the Kalman Filter. CBX 92-39, 1992
7 Kalman R E. J. Basic Eng., 1961, **83**: 95—107
8 Frühwirth R. Nucl. Instrum. Methods A, 1987, **262**: 444—450
9 Billoir P. Nucl. Instrum. Methods A, 1984, **225**: 352—366
10 Frühwirth R, Todorov T, Winkler M. Track Fitting Method in ORCA. CMS IN 058, 2002
11 Badalà A et al. Nucl. Instrum. Methods A, 2002, **485**: 15—22
12 Rutger van der Eijk et al. Performance of the LHCb OO Track Fitting Software. LHCb note 086, 2000
13 Belle Tracking Group. Charged Particle Tracking in Belle. Belle Note 327, 2000
14 Frühwirth R. Computer Physics Communications, 1997, **100**: 1—16
15 Frühwirth R. Track Reconstruction in the CMS Tracker. CMS CR 014, 2005
16 Frühwirth R, Todorv T, Winkler M. J. Phys. G: Nucl. Part. Phys., 2003, **29**: 561—574
17 Miyake H, Trabelsi K. Use of Kalman Filter for Muon Identification. Belle Note 298, 2000
18 Brown R G. Introduction to Random Signal Analysis and Kalman Filtering. New York: Wiley Press, 1983
19 Welch G, Bishop G. An Introduction to the Kalman Filter. TR 95-041, 1995
20 Frühwirth R, Regler R M, Bock R K, Grote H, and Notz D. Data Analysis Techniques for High-Energy Physics. Cambridge University Press, 2000
21 HUANG Shi-Ke. Magnetic Field Mapping in the BESIII Solenoid. PhD Thesis. 2008 (in Chinese)
22 Ohnishi Y. Track Parameterization. Belle Note 148, 1997
23 Harr R. IEEE Trans. Nucl. Sci. 1995, **42**(3): 134—147
24 WU Ling-Hui. Study of the Offline Calibration for the BESIII Drift Chamber and the Beam Test of a Protype. PhD Thesis. 2008 (in Chinese)
25 YAO W M et al. Journal of Physics G, 2006, **33**(1): 258—270
26 Avery P. The Charged Particle Energy Correction in CLEO. CBX 92-40, 1992
27 Brown D N, Charles E A, Roberts D A. The BaBar Track Fitting Algorithm. In Proceeding of Computing in High Energy Physics Conference, Padova, 2000
28 Kutschke R, Ryd A. Billoir Fitter for CLEO II. CBX96-20, 1996
29 Agostinelli S, Allison J et al. Nucl. Instrum. Methods A, 2003, **506**: 250—303
30 http://belle.kek.jp/∼karim/